ELSEVIER

Journal of Hazardous Materials 46 (1996) 241–252

JOURNAL OF HAZARDOUS MATERIALS

Wind tunnel simulation of ammonia gas release transport processes

J.N.E. Papaspyros, P.N. Papanicolaou, E.G. Kastrinakis, S.G. Nychas*

Department of Chemical Engineering, Aristotle University of Thessaloniki, University Box 453, GR-540 06 Thessaloniki, Greece

Received 6 May 1994; accepted 27 January 1995

Abstract

This work reports on experimental data and generalized correlations, which display the modification of a scalar field by the presence of obstacles. The data were obtained by means of a triple hot-wire probe in a wind tunnel. The global picture of the flow was visualized and recorded by a high-speed video system. The flow studied was a buoyant jet in a cross wind. This flow simulates an accidental ammonia release from a pressurized containment. The obstacle is found to enhance scalar turbulent dispersion and mixing. The simulated ammonia plume exhibits similar dynamic behavior with and without the obstacle, obtaining a self-similar state at distances downwind predicted by dimensional arguments. The scalar probability density functions display deviations from Gaussian distribution, depending upon their distance from the jet center. The data support a gradient transport hypothesis modeling. Recirculation patterns contributing to the entrainment processes were identified in the near wake of the obstacle.

Keywords: Ammonia release; Turbulent transport terms; Jet in cross flow; Model validation; Obstacle effect on scalar dispersion

1. Introduction

An accidental ammonia release from pressurized containment will constitute a two-phase mixture, subjected to ambient conditions and atmospheric wind motions. At some distance downwind ammonia will become gaseous, reaching ambient air temperature and will behave like a positively buoyant jet in a cross flow. The processes of ammonia dispersion and mixing will be influenced by the presence of buildings, tanks, etc. Knowledge of ammonia dispersion and mixing characteristics is necessary for plant design and accurate risk and hazard assessment purposes.

* Corresponding author. Tel.: 0030 (031) 996231. Fax: 0030 (031) 206138.

SSDI 0304-3894(95)00076-3

The Laboratory of Chemical Engineering Fundamentals is carrying out a wind tunnel simulation of the transport processes, related to the dispersion and mixing of gases and vapor clouds in an industrial environment. The work presented here is part of the project sponsored by the Commission of the European Communities: 'Research on the Dispersion of Two-Phase Flashing Releases – FLADIS'.

We present herein data and generalized correlations that display the modification of the scalar field (simulated ammonia concentration) by the presence of obstacles. A simple case, which could form the basis for modeling of more complex geometries, is examined, namely the modification of ammonia dispersion and mixing by a single three-dimensional structure.

2. The flow under investigation

Scalar measurements involve heat as a contaminant, since the Schmidt and Prandtl numbers for gases are of order one. The flow under investigation is sketched in Fig. 1. A buoyant jet of hot air simulates gaseous ammonia motion, while the atmospheric wind motions are simulated by a cross flow in our wind tunnel. The jet is pointing vertically upwards and it is normal to the cross flow. The jet nozzle is at the same level with a flat plate, which simulates a smooth terrain. A vertical cylinder simulates a single three-dimensional structure.

The dynamic characteristics of heated air jets are generally parameterized in terms of their initial specific (i.e., per unit mass) flux of mass, momentum and buoyancy [1]:

$$Q = \left(\frac{\pi D^2}{4}\right) W_0,$$

$$M = QW_0, \tag{1}$$

$$B = \frac{Q(\rho_\infty - \rho_0)g}{\rho_0},$$

where Q is the volume rate of flow or specific mass flux, M is the specific momentum flux and B is the specific buoyancy flux. The initial jet Richardson number is defined as

$$Ri = \frac{QB^{1/2}}{M^{5/4}}. \tag{2}$$

It is now well documented, by both dimensional arguments and experimental evidence [2], that the major flow characteristics, including jet trajectory and scalar decay, may be determined by means of Richardson number and velocity ratio, R:

$$R = \frac{W_0}{U_\infty}. \tag{3}$$

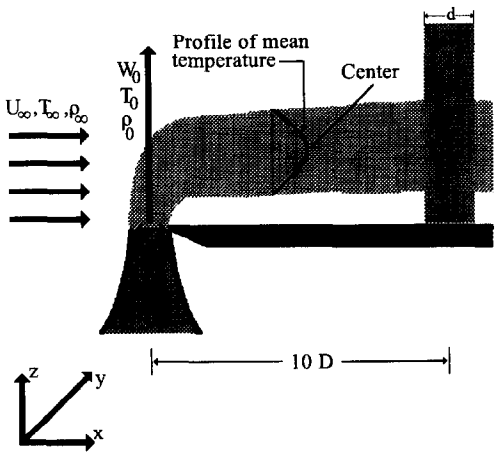

Fig. 1. The flow under investigation.

The buoyant jet in the measurements reported here is expected to develop a plume-like behavior at distances from nozzle exit of order

$$z_c = \left(\frac{M^2}{BU_\infty}\right)^{1/3}. \tag{4}$$

Characteristic values in this work refer to the jet center, defined as the point in the plane of symmetry of the jet, where the mean temperature (or, correspondingly, ammonia concentration) takes maximum values. This point is shown in Fig. 1, and will be denoted by subscript 'c'.

3. Experimental

The experimental apparatus used consists of a wind tunnel, a flat plate, a small heated jet and a vertical cylinder. The wind tunnel is an open circuit tunnel of suction type, with a flow straightening honeycomb positioned in the effuser section and an axial flow fan at the end of the diffuser section. The fan is driven by a DC motor, obtaining maximum velocity of 28 m/s. The power is provided by a voltage stabilizing power unit, while the motor operating voltage is controlled by a rheostat for adjustment of the fan rotation frequency (and wind tunnel velocity). The 2 m long test section has a 30 cm × 30 cm cross section and is made of mahogany, with lucite removable windows. The traversing mechanism and sensors are mounted on to an overstructure supported by the lab ceiling, so that the vibration induced by the fan or tunnel resonance is avoided. Precision positioners (of accuracy 10 μm) were used to position the sensors within the flow field. Free stream turbulence was lower than 0.5%.

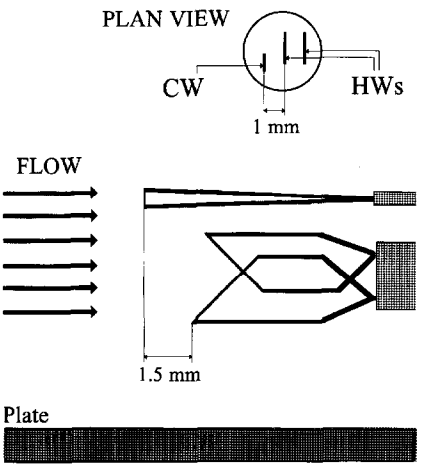

Fig. 2. The probe used (not to scale).

The flat plate is made of 2 cm thick aluminum, and has a sharp leading edge with bottom slope 1:5 and side slopes 1:1. The small jet is positioned at the end of a 1.27 cm PVC pipe, inside of which the air heating element (a wire resistor, connected to a power supply) is mounted. Right after the heating section there is a thermistor, connected to a temperature controller. This system performs a feedback stabilization of the jet temperature at the nozzle exit, typically within $\pm 0.5\,^{\circ}C$. The air reaches the removable jet nozzle through a section filled with wire sponge, that homogenizes the flow and dissipates the turbulence. The jet nozzles used in this work were 0.265, 0.40, 0.55, 0.75 and 1 cm in diameter. The cylinders used were made of hard PVC with low thermal conductivity, so that heat absorption by their surface was minimized. Cylinders of two different diameters, 2 cm and 3 cm, were used.

The measurements reported here were acquired by means of a triple wire probe. An X-wire DISA 55P61 probe (platinum-plated tungsten wires, 1.25 mm in length, 5 μm in diameter, 1 mm sensor separation), measuring two components of instantaneous velocity, and a DISA 55P31 resistance thermometer (platinum wire, 400 μm in length and 1 μm in diameter), measuring temperature, were brought in close proximity, as shown in Fig. 2. This technique has been used by Lienhard V and Van Atta [3]. The probes were oriented within the flow field in such a way, as to ensure that the thermal wake of the hot wires had a negligible influence on the cold wire. The total measuring volume of the triple probe was $2 \times 1.5 \times 1.5\ mm^3$, with the larger dimension in the direction of the velocity component which was not measured. The probe configuration provided the instantaneous simultaneous measurements of one Reynolds stress (uw, where u corresponds to the streamwise velocity fluctuation, that is deviation from time averaged mean value, and w corresponds to the vertical velocity fluctuation) and two turbulent scalar fluxes (uT' and wT', where T' is the temperature fluctuation). The triple probe was operated with AN-1003 anemometry circuits. The current fed to

the cold wire was 0.265 mA and the overheat ratio of the hot wires was 30%. The frequency response of the circuits (−3 dB point) extended to about 20 kHz, that was well above our sampling frequency (4 kHz). The output noise of the circuits had an rms value up to 20 mV, in a full scale of 20 V. The drift of the circuits was negligible. The A/D converter used was a 16-bit unit, type Data Translation DT2809, equipped with sample-and-hold circuits, thus ensuring simultaneous measurements from up to 8 channels.

The velocity sensors were calibrated by a specially developed technique, accounting for temperature changes and their effect on X-wire output voltages. Simultaneous temperature and velocity signals were acquired during heating of a calibration jet unit. The response of the triple probe to gradual heating was thus recorded and the acquired information was combined to produce a calibration data base. This procedure provided calibrations stable over long time periods (more than two weeks) and it lasted less than an hour.

The combined error in the temperature measurements reported here is estimated to be up to $\pm 1\%$, whereas the error in the velocity measurements is estimated to be up to $\pm 2\%$ for the longitudinal velocity component and up to $\pm 3\%$ for the vertical velocity component. Larger errors are expected in the region right behind the cylinder, where strong recirculation occurs (see Section 4.6). For the data closer to the lee of the cylinder (at $x = 1.5$ d from the center of the cylinder) the temperature is overestimated by 10%.

The point measurements acquired by the triple probe were coupled with flow visualization and subsequent image recording and analysis; the latter provided a global picture of the flow. The buoyant jet air feed was passed through a smoke generator, where smoke of burning incense was injected into the air, thus visualizing the jet flow. A high-speed video system model NAC HSV-400 videotaped the visualized flow at 200 and 400 pictures per second. This system consists of a high sensitivity, high-resolution three-tube color camera with built-in high speed (up to 10 kHz) shutter, a high-intensity strobe, a video tape recorder, a monitor simultaneously displaying the image being recorded and supplementary accessories which provide image analysis capability.

4. Results and discussion

Simultaneous measurements of local instantaneous values of temperature and two velocity components (U and W) were performed in two phases: (i) without the obstacle and (ii) with the obstacle present. During the first phase, a wide range of Richardson number and velocity ratio values was covered, thus enabling the determination of a reference basis that would elucidate the effect of the obstacle. The Richardson number varied from 0 (jet-like behavior) up to 0.1 (strongly buoyant jet), while the velocity ratio, R, ranged from 2 to 8. The measurements covered distances from 10 D up to 100 D downstream of the jet nozzle exit; they were performed at each station along the jet line of symmetry and/or along a line passing through the jet center and parallel to the flat plate ('cross' measuring pattern). Complete scans of the

jet cross section were performed at several stations. During the second phase of measurements, that is with the cylinder present, a representative case was selected which would better simulate ammonia release. The Richardson number corresponding to the test case was 0.1 and the velocity ratio was 2.5. The uniform cross flow velocity had a value of 1 m/s and the characteristic length scale z_c was about 9 cm. The jet nozzle used during this test case had a $D = 1$ cm. Cylinders of $d = 2$ cm and $d = 3$ cm were used, placed with their axis at approximately $x = 10$ cm downstream of the jet nozzle exit. The jet width, before impingement upon the obstacles, was of the order of magnitude of the two obstacle diameters used. The top edge of the cylinders was always above the simulated cloud. The same patterns as in the first phase were used (i.e., 'crosses' and complete scans) and distances from $x = 1.5$ d up to $x = 44$ d downstream of the center of the cylinder were covered. The Reynolds number for all the experiments of both phases, based on the jet nozzle diameter, ensured fully developed turbulence, varying from 1400 up to 3200.

4.1. Buoyant jet trajectory and width

The prediction of the buoyant jet trajectory is very important for safety analysis. Several correlations existing in the literature predict this major flow characteristic, with somewhat contradictory results. One of these correlations, proposed by Kamotani and Grebber and cited and discussed in Demuren [4], was found to agree with our data. The jet trajectory was not significantly affected by the presence of obstacles for the case studied. The jet width was widened by approximately 20% in the near wake of the cylinders.

4.2. Scalar decay and degree of mixing

The dimensionless mean temperature along the jet centerline is plotted in Fig. 3 as a function of the downstream distance from the jet nozzle, normalized with z_c. This functional dependence, usually referred to as 'centerline temperature decay', simulates the decrease of ammonia concentration along the jet centerline. The data measured in the absence of obstacle agree with other data in the literature [5]. The scalar decay for $x < z_c$ exhibits a $\frac{2}{3}$ slope, changed to a $\frac{4}{3}$ slope for $x > z_c$ when the buoyant jet behavior becomes plume-like. This dependence is predicted by dimensional arguments [2].

The presence of obstacles greatly enhances the turbulent mixing of the scalar, reducing mean temperature (increasing decay) by a factor of 3. This effect is a typical one [6]. The scalar decay behind the obstacle displays a behavior similar to the one in the absence of obstacle, and develops the same self-similar behavior. This important aspect, together with the large number of directly measured parameters, renders the present data appropriate for validation of computational models predicting the dispersion and mixing of clouds in an industrial environment. For the thicker cylinder used slightly larger decays were observed. The data right behind the obstacle (at distances up to $x = 8$ d from the center of the cylinder) display a lower increase of decay rates. This fact is attributed to recirculation occurring in the near wake of the

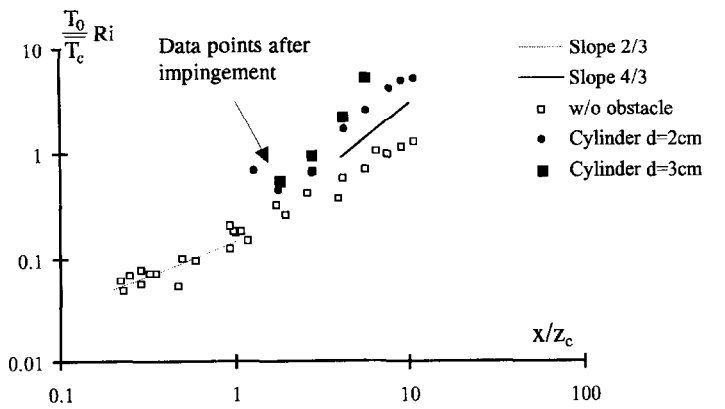

Fig. 3. Decay of centerline temperature.

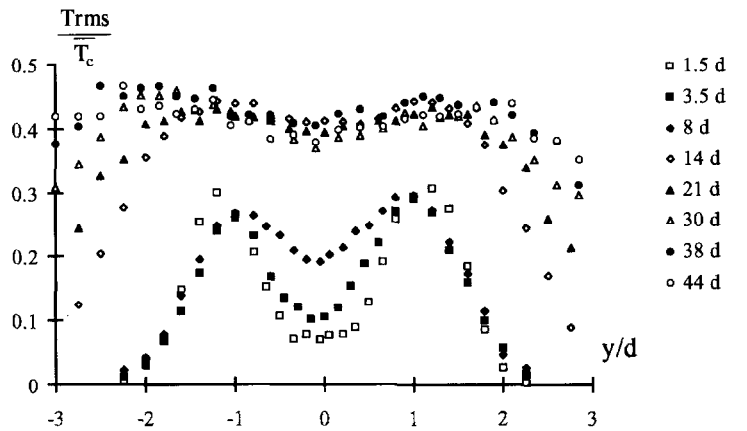

Fig. 4. Scalar rms across the buoyant jet, for $d = 2$ cm; $Ri = 0.1$.

cylinder. The recirculation (i) advects hot air from downstream back to the lee of the cylinder and (ii) causes temperature overestimation, as hot wakes from the velocity sensors (hot wires) contaminate the signals of the temperature sensor.

The maximum instantaneous values of temperature time signals and temperature rms values along the jet centerline follow the trend of mean temperature, displaying the same decay rule, as was reported by Papanicolaou and List [1] for plain turbulent jets and plumes (i.e., without cross flow).

The enhancement of turbulent scalar dispersion and mixing caused by the presence of the obstacle is depicted in Fig. 4; here, the normalized scalar rms values along a line passing through the jet center and parallel to the flat plate are plotted for several measurement stations downstream of the obstacle. The intensity of turbulent scalar

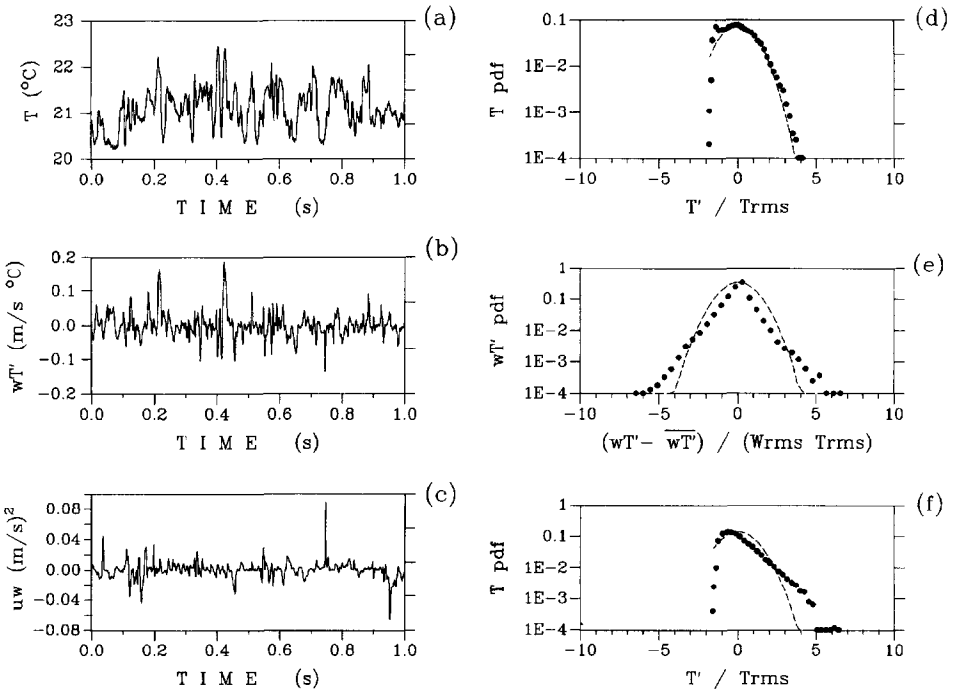

Fig. 5. Example of time signals and probability density functions.

mixing can be inferred from the T_{rms}. Two regions are clearly seen. The first region is the cylinder near wake ($x < 10\,d$ downstream of the cylinder center) which is characterized by enhanced turbulent scalar dispersion near the scalar rms inflection points and higher degree of mixing around the centerline of the jet. The second region ($x > 10\,d$) displays enhanced mixing across the whole jet cross section. The first region corresponds to the recirculation zone documented by the visual study. The normalized T_{rms} values in the second region are typical of plume-like behavior [2]. The transition between these two regions is rather abrupt.

4.3. *Time signals and probability density functions*

Representative time signals, acquired at $x = 21$ d downstream of the center of the 2 cm diameter cylinder, are depicted in Fig. 5. Graphs (a) and (d) are the temperature time signal and corresponding probability density function (pdf) at the center of the jet. Graphs (b) and (c) are the simultaneously with (a) directly measured time signals of vertical turbulent heat flux and Reynolds stress *uw*, whereas graph (e) is the corresponding pdf of (b). Graph (f) is the temperature pdf at a point in the hot jet/cold air interface. The long tail of this pdf is of great importance for safety analysis (the dashed lines correspond to the pdf of a normal distribution).

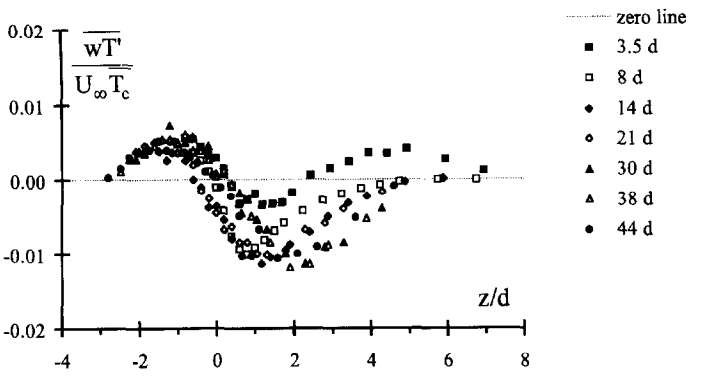

Fig. 6. Vertical turbulent heat flux along the jet line of symmetry ($y = 0$), for $d = 2$ cm; $Ri = 0.1$.

4.4. Turbulent transport terms

As already noted, during the present study two turbulent heat flux terms and one component of Reynolds stress tensor were directly measured. This information is valuable for validation of mixing and dispersion models in environmental flows. The properly normalized vertical turbulent scalar transport term along the jet line of symmetry is plotted in Fig. 6 for several distances downstream of the center of the 2 cm diameter cylinder. The two regions already identified can be recognized in this figure as well. The flux term develops a self-similar profile in the second region ($x > 14$ d). This profile supports a gradient transport hypothesis model for the vertical turbulent heat transport term, $\overline{wT'}$. The large extent of the recirculation zone is implied by the regions where the term $\overline{wT'}$ is nonzero.

4.5. Scalar contour map

Detailed scans of jet cross section were performed at several measurement stations, providing a more complete picture of the flow field. As an example, the temperature contour map at a distance $x = 3.5$ d downstream of the center of the 2 cm diameter cylinder is depicted in Fig. 7. The large extent of the recirculation region, already discussed, is seen again in this picture.

4.6. Visual study

In order to obtain a global picture of the flow field a visual study was undertaken. The most important observations are depicted in Fig. 8 and are the following:

- an entrainment process, enhanced by the recirculation patterns in the near wake of the cylinder, was observed to be responsible for the vertical spreading of the jet.

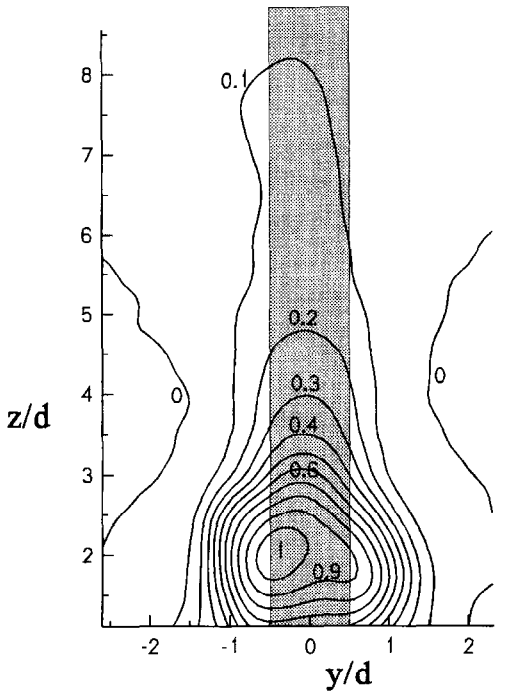

Fig. 7. Typical contour map of the time averaged scalar, normalized by the maximum value of the cross section.

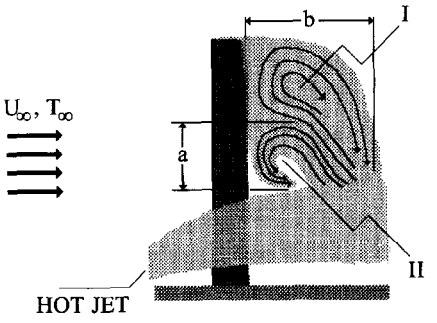

Fig. 8. Schematic of recirculation zone.

- a three-dimensional flow structure (I in Fig. 8), produced by the well-known trailing vortex behind the obstacle [7, 8], was observed in the present flow as well.
- in addition, a recirculating flow motion (II in Fig. 8) was observed to contribute to the vertical spreading of the jet.

Characteristic scales were determined from the video recordings. Two such length scales *a* (of the order of 2 to 3 d) and *b* (of the order of 3 to 4 d) are shown in Fig. 8.

5. Conclusions

The main conclusions of the present work are the following:

- the major flow characteristics of a simulated ammonia cloud subjected to an atmospheric wind motion, with and without obstacles, may be determined by two dimensionless numbers, namely a Richardson number and a velocity ratio. The flow develops the same self-similar behavior in the presence and absence of obstacles. The presence of cylindrical obstacles, having a diameter comparable to the cloud width, increases the scalar decay rate by more than three times.
- the vertical turbulent scalar transport term, at some distance downstream of the obstacles, develops a self-similar profile. This profile supports a gradient transport hypothesis model.
- the scalar probability density functions display deviations from Gaussian distribution, depending upon their distance from the jet center. Exponential-type distributions with long tails were also observed.
- large-scale recirculation motions, observed in the near wake of the obstacle, enhance entrainment and vertical spreading of the jet.

Nomenclature

B	jet specific buoyancy flux at the exit of the nozzle (Eq. (1))
d	diameter of the cylindrical obstacle (Fig. 1)
D	jet nozzle diameter (Fig. 1)
g	gravitational acceleration
M	jet specific momentum flux at the exit of the nozzle (Eq. (1))
Q	jet volume flux at the exit of the nozzle (Eq. (1))
R	jet exit to cross flow velocity ratio (Eq. (3))
Ri	jet Richardson number at the exit of the nozzle (Eq. (2))
T_0	jet excess (above T_∞) temperature at the exit of the nozzle
$\bar{T}_c$	mean excess (above T_∞) temperature at the center of the jet (Fig. 1)
T_∞	cross wind uniform ambient temperature (Fig. 1)
U	local instantaneous streamwise velocity
U_∞	cross wind uniform velocity (Fig. 1)
u	fluctuation of U
W	local instantaneous vertical velocity
W_0	jet velocity at the exit of the nozzle (Fig. 1)
w	fluctuation of W
z_c	characteristic length scale (Eq. (4))

Greek symbols

ρ	density
ρ_0	jet density at the exit of the nozzle
ρ_∞	ambient fluid density

Superscripts and subscripts

$(^{-})$	time averaged mean value of a quantity
$()_c$	centerline value of a quantity
$()_0$	value of a jet quantity at the exit of the nozzle
$()_\infty$	value of an ambient and cross flow quantity

Acknowledgements

This work has been supported by the EEC STEP program on Major Technological Hazards, under contract #STEP-PL-900597.

References

[1] P.N. Papanicolaou and E.J. List, Int. J. Heat Mass Transfer, 30(10) (1987) 2059.
[2] H.B. Fischer, E.J. List, R.C.Y. Koh, J. Imberger and N.H. Brooks, Mixing in Inland and Coastal Waters, Academic Press, New York, 1979.
[3] J.H. Lienhard V and C.W. Van Atta, J. Fluid Mech., 210 (1990) 57.
[4] A.O. Demuren, in: N. Cheremisinoff (Ed.), Encyclopedia of Fluid Mechanics, Vol. 2, Gulf Publ. Co., Houston, 1986, p. 430.
[5] V.H. Chu and M.B. Goldberg, J. Hyd. Div., 100 (1974) 1203.
[6] N.J. Duijm and D.M. Webber, J. Loss Prev. Process Ind., 7(2) (1994) 118.
[7] W.H. Snyder, Downwash of plumes in the vicinity of buildings. A wind-tunnel study, presented at the NATO Advanced Research Workshop: Recent Research Advances in the Fluid Mechanics of Turbulent Jets and Plumes, Viana do Castelo, Portugal, 1993.
[8] P.J. Mason and B.R. Morton, J. Fluid Mech., 175 (1987) 247.